Lasers in Manufacturing Conference 2021

Vapor plume behavior during a standalone laser pulse on the dissimilar aluminum/titanium interface: high-speed imaging with 810 nm band-pass filter

Manoj Raja Kumar[a,*], Iryna Tomashchuk[a], Jean-Marie Jouvard[a], Mélanie Duband[a]

[a]*Laboratoire Interdisciplinaire Carnot de Bourgogne, UMR CNRS-6303, Université de Bourgogne Franche-Comté, 12 rue de la Fonderie, 71200 Le Creusot, France*

Abstract

The understanding of plume behavior in dissimilar laser welding is little studied and can bring an insight to the concurrent vaporization process and keyhole dynamics. The present study is dedicated to the high-speed imaging and post-mortem characterization of a standalone Yb:YAG laser pulse on aluminum A5754/titanium interface with different offsets to the joint line. Plume morphology, dimensions, orientation and propagation velocities were characterized basing on the videos performed with an 810 nm band-pass filter. The main observed feature of the plume was its pronounced initial inclination towards aluminum side, accentuated by the beam offset on A5754 and reduced by the offset on titanium, followed by a progressive redressing resulting in a close to vertical jet. This behavior was attributed to the domination of the vapor jet from titanium side over that of aluminum side during the evolution of keyhole curvature. SEM observations of the melt were found in agreement with this statement.

Keywords: laser welding; vapor plume; dissimilar welding; high-speed imaging.

1. Introduction

Laser welding of dissimilar metallic materials has numerous advantages over conventional welding techniques such as precise control of melted zone composition, smaller HAZ, high welding speed, the non-contact feature compared to conventional welding techniques, etc. Many works are dedicated to the optimization of dissimilar weld composition in view of better mechanical properties. However, research focus on the physics of interaction of laser beam with dissimilar joint is relatively rare, especially on the aspect of keyhole dynamics. The pronounced mismatch in physical properties of the joined metals leads to the

* Corresponding author.
E-mail address: Manoj.Raja-Kumar@u-bourgogne.fr .

formation of the asymmetrical keyhole partially or totally shifted from the joint line, which highly affects the joint composition and quality (Tomashchuk et al., 2017).

The analysis of vapor plume produced during a high power laser-metal interaction allows better comprehension of keyhole dynamics. High speed imaging with use of different pass-band filters is one of the most accessible tools for online monitoring of laser-material interaction. In the laser welding of 5083 aluminum alloy, the correlation was observed between the oscillation in plume velocity and the keyhole dynamics and morphology (Huang et al., 2020). The correspondence between the plume inclination and the angle of vaporization front of the keyhole was observed for the welding of stainless steel (Brock et al., 2014).

In our previous work, dedicated to the continuous laser welding of titanium to aluminum alloy A5754, the pronounced periodical inclination of the vapor plume towards aluminum side of the joint was correlated with the presence of solidification patterns observed on the joint surface (Raja Kumar et al., 2020). The existence of two competing jets was attributed to the temporal evolution of the keyhole walls. The unstable keyhole wall from aluminum side was periodically opening along with the inclination of the jet, whereas between these inclinations the vertical direction of the jet was associated with the keyhole digging within a new portion of titanium side of the joint. The beam offset on aluminum side, where the keyhole has unstable behavior, induced partial plume extinction and intense spattering, whereas the formation of bright stable plume associated with stable keyhole was observed for the beam offsets on titanium.

For better comprehension of the behavior of the keyhole shared between two materials in view of existing mismatch in physical properties, in the present study, the high speed imaging of the vapor plume is performed in the case of a short standalone laser pulse. The plume induced in individual materials and in dissimilar titanium/aluminum joints with different beam offset from the joint line is characterized by automated image processing using ImageJ software. Additionally, the post-mortem characterization of the impact zones by SEM-EDS is performed.

2. Experimental procedure

2.1. Plume observation experiments

Trumpf TruDisk 6001 Yb:YAG laser (λ = 1030 nm) with a spot diameter of 600 µm was used to produce 2 kW, 2 ms pulses on the metal plates. The experiments were done with rectified 3 mm thick plates of commercially pure titanium T40 and A5754 aluminum alloy (Table 1) after cleaning the plates with ethanol. No protective gas flow was used. Laser pulses were performed on standalone materials and in dissimilar combinations. The beam offset from the joint line (Δ) on titanium was considered as positive, and on A5754 as negative (Fig 1a). For the dissimilar combinations, five different laser spot offsets from the joint line were applied: -200 µm, -100 µm, 0 µm, +100 µm and +200 µm. Each experimental condition was repeated thrice.

Table 1. Chemical composition and main physical properties of used materials.

Materials	**A5754 aluminum alloy**	**Ti T40**
Elemental composition (wt.%)	2.6 Mg, 0.5 Mn, 0.4 Si, 0.4 Fe, 0.3 Cr, 0.15 Ti, 0.2 Zn, 0.1 Cu	99.9 Ti
Absorptivity at 1030 nm at 20°C	15%	40%
Melting point (K)	883-902	1941
Boiling point (K)	2792	3560
Thermal diffusivity (10^{-6} m²/s)	98.8	9.4

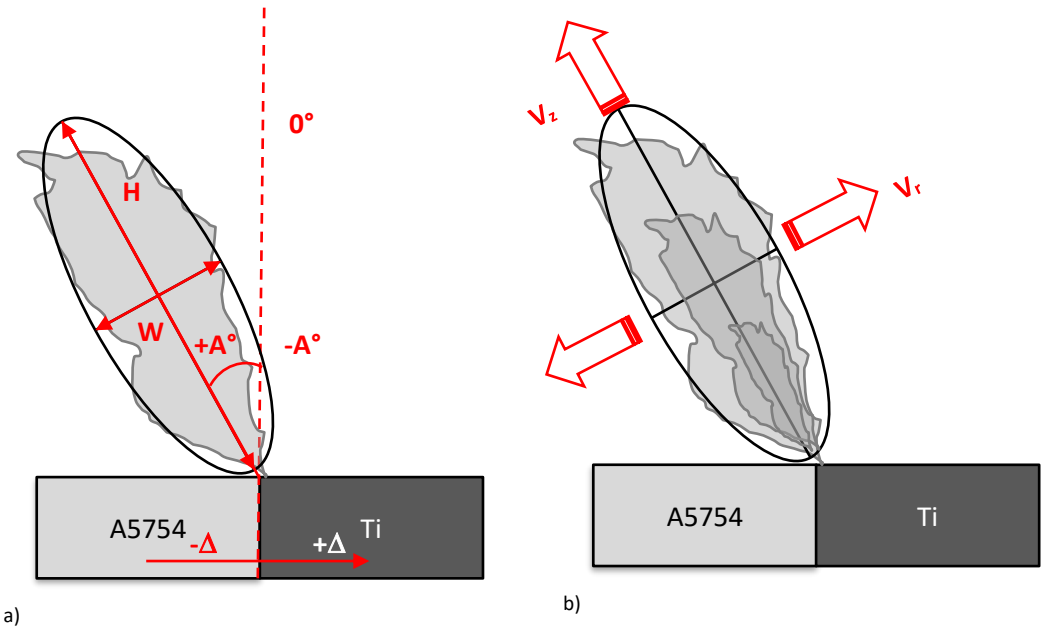

Fig. 1. Schematic of geometrical characteristics of the vapor plume (a) and the directions of axial and transversal expansion rates (b).

High speed camera Phantom V9.1 with a CMOS sensor was used to capture the front view of the vapor plume through an 810 ± 3 nm optical band pass filter with full width at half maximum of 10 ± 2 nm, from the distance of 65 cm. At this wavelength, only the continuous thermal emission of the vapor plume is perceived by the camera. The frame rate was 6400 fps over a zone of capture with area 15 mm x 15 mm at resolution 480 x 480 pixels with an exposure time of 120 µs. All acquisitions were made with the same parameters of the camera. Additional illumination of the welding scene was not necessary, as the plume naturally appears luminous on the chosen filter wavelength.

Post-mortem characterization of the impact zones was done by JEOL JSM-6610LA electron microscope equipped with an EDS analyzer.

2.2. Image processing and analysis

The post-processing treatment of the images was performed using ImageJ software (Schneider et al., 2012). All the videos were cropped manually to remove the melted zone that was partly visible and bright, so only the vapor plume was left to be treated. Every experiment constituted of a stack of 13 images, the gray values of which were normalized by equalizing the stack histogram.

After the processing, the spatial characteristics of the plume were analyzed. Thresholding of the normalized stacks with a lower limit of 128 gray value (50% of the maximum) was performed first in order to eliminate the background noise, very diffuse parts of the plume and the zones illuminated by spatters and electronic blooming. This operation enabled image segmentation into clear plume and dark non-plume zones, which subsequently allowed measurement of the image statistics. Although the plume constitutes an irregular profile, it can be characterized in a quantitative manner through a series of variables using a better approximation to the shape of the profile. The technique applied to the plume profile was done by assuming that the plume image constitutes a uniform distribution of points bounded by the perimeter of the profile that

resembles an ellipse. This measure produces the length of the major axis, the minor axis and the angle of the ellipse inclination, from which the plume height (*H*), the plume width (*W*) and the inclination angle with respect to the verticality (*A°)* were inferred (Fig 1a). The obtained results were concordant with the dimensions of the plume manually measured using the untreated videos.

The uncertainty associated to the plume dimension analysis was considered in the following way. For the frame rate of 6400 fps, the two consecutive images *n* and *n+1* are separated by the time lapse t_{n+1}-t_n of 156 µs, which brings the incertitude of ±78 µs to the interaction time corresponding to each image. The initial times for each frame and the respective horizontal error bars were used for data representation (Fig 3). The dimensions of the plumes were evaluated on three videos for each experimental condition, and the fluctuations of *H*, *W* and *A°* were represented as the range ±(*Max-Min*)/2. The average values for each frame and the respective vertical error bars were used for data representation (Fig 3).

The axial (*Vz*) and transversal (*Vr*) velocities of plume expansion (Fig 1b) were evaluated basing on the average values of *H* and *W* according to the expressions $(H_{n+1}-H_n)/(t_{n+1}-t_n)$ and $(W_{n+1}-W_n)/(t_{n+1}-t_n)$.

3. Results and discussion

3.1. General observations on plume behavior and morphology

The use of 810 nm filter which allows only the continuous thermal emission of the vapor plume led to very dull images for standalone aluminum alloy (left column on Fig 2) and to very bright plume images for titanium (right column on Fig 2). The vapor plumes of the standalone materials were symmetrical to the vertical axis. The aluminum alloy plume formed a stagnating spherical shape and the titanium plume formed a mushroom-like shape that rapidly transformed into an intense vertical jet, with some turbulent effects setting in near the end of the pulse. Such difference in plume behavior can be attributed to poor absorption, high reflectivity and high thermal conductivity of aluminum compared to titanium, as well as to the mismatch of their vaporization temperatures (Table 1). Therefore, laser irradiation of the titanium side of the dissimilar joint would make a major contribution to the local heat transfer.

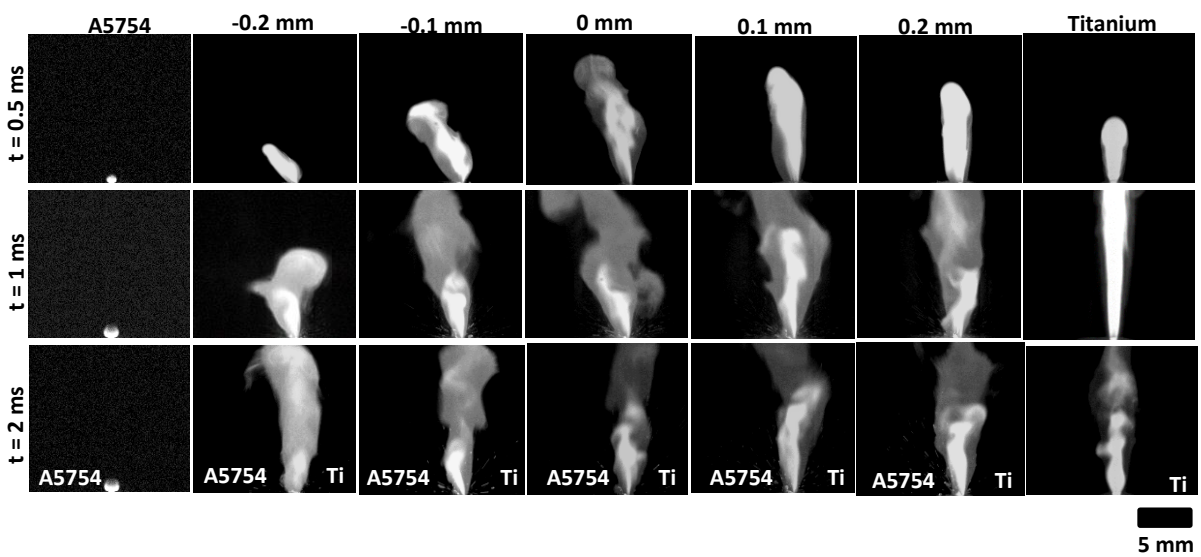

Fig. 2. The morphologies of the plume formed above standalone materials and dissimilar joints with different Δ.

Laser pulse on the dissimilar joints produced the plumes of intermediate luminosity. The plumes were more turbulent and diffuse than in standalone titanium, and revealed the preferential inclination on aluminum side that depended on the position of the laser spot with respect to the joint line and on the interaction time. The beam offset on aluminum accentuated the inclination of the plume and reduced its height, whereas the beam offset on titanium produced higher and less inclined plumes.

The process of dissimilar plume expansion can be divided into three stages: initiation, stagnation and recompensing. During the initiation stage ($t < 0.5$ ms, top row on Fig 2), the plume is compact, it quickly develops the inclination on aluminum and undergoes rapid expansion. During the following stagnation stage ($0.5 \text{ ms} < t < 1$ ms, middle row on Fig 2), the dissimilar vapor plume becomes more diffuse, slows down the expansion, but conserves the inclination on aluminum side close to the angle achieved during the initiation phase. The final stage of recompensing starts at $t > 1$ ms, when the plume progressively approaches verticality (bottom row on Fig 2).

3.2. Plume dimensions, orientation and expansion velocities

The analysis of plume height (Fig 3a) showed that the spherical plume observed in standalone aluminum alloy conserved the height below 1 mm during all pulse time, which corresponds to a heat transfer equilibrium between heat inflow by laser radiation and heat loss through evaporation. On the other hand, the plume in standalone titanium was rapidly expanding up to 14 mm and sometimes exceeded the dimensions of the observation zone. For the dissimilar joints, it can be seen that *H* increases progressively as the laser spot is displaced from the aluminum side to the titanium side. In case of pure aluminum and maximal tested beam offset on aluminum (-200 µm), the height of the plume undergoes a temporary depression that appears after the expansion stage. This temporary decrease of plume intensity can be attributed to the evacuation of alumina layer that strongly absorbs the laser radiation until it is replaced by the highly reflective liquid aluminum, associated with the temporary decrease of surface temperature. For other beam offsets, the height of the plume remains little below that of standalone titanium, which underlines its important contribution to the vaporization process.

The width of the vapor plume (Fig 3b) is superior to the laser spot diameter (600 µm) in all experiments. Standalone aluminum produces a plume of a minimal width below 2 mm, when standalone titanium jet reaches the maximal width of 3 mm. However, the dissimilar joints produce much wider plume (up to 6 mm) for all tested beam offsets. This can be attributed to the mixing of competing Al-rich and Ti-rich vapor jets enhancing the turbulent effects. For the experiments with beam offsets of 0, -100 µm and +100 µm, the decrease in width is observed near the end of the pulse, as the plume inclination reduces, and the competing jets join into one unidirectional jet.

The analysis of plume inclination angle in the dissimilar joints (Fig 3c) showed that for all tested beam offsets, the plume inclination grows during the initiation stage, reaches its maximum between 0.5 and 1 ms and progressively disappears after $t > 1$ ms. For the same interaction times, the magnitude of the inclination angle is proportional to the beam displacement from titanium to aluminum. The maximal observed inclination angle diminishes from 55° to only 6° with increase of beam offset from – 200 µm to 200 µm (Fig 4). The minimal beam inclination, observed by the end of the pulse, is close to 0°.

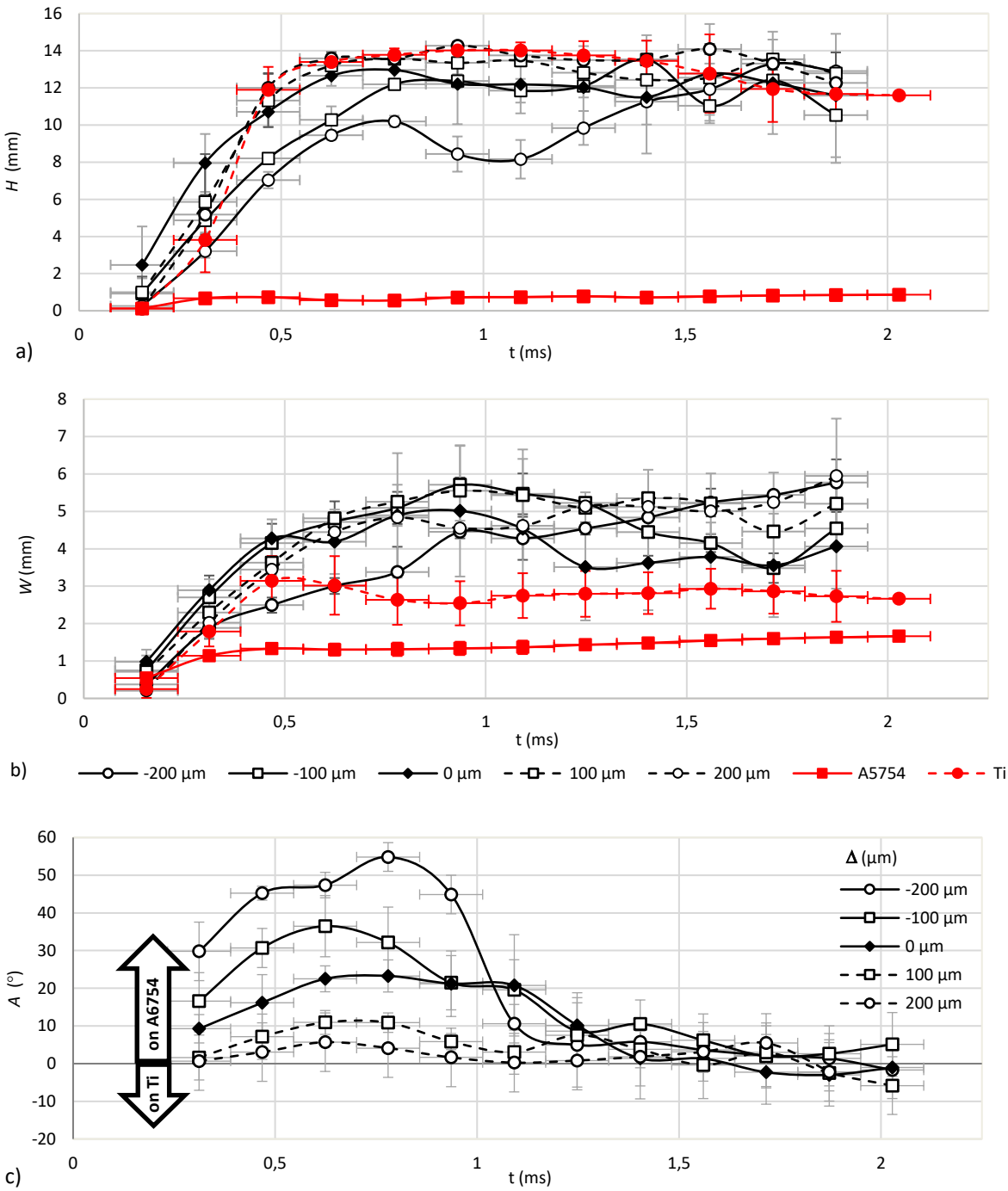

Fig. 3. Plume axial height (a), transversal width (b) and inclination angle (c) during the 2 ms pulse on standalone materials and dissimilar joints with different Δ.

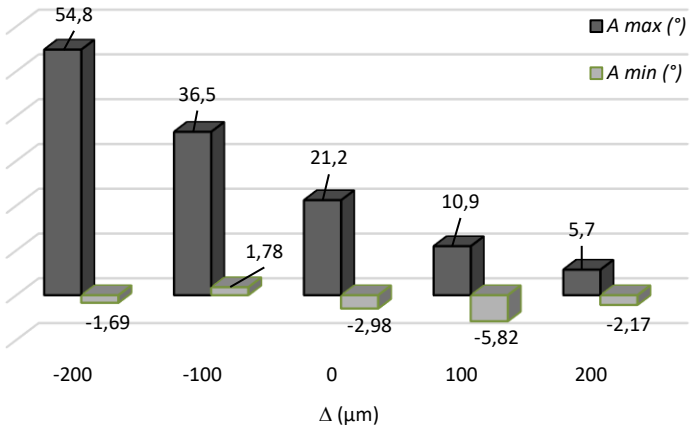

Fig. 4. The evolution of maximal and minimal observed inclination angles for the dissimilar joints with different Δ.

The evaluation of axial (*Vz*) and transversal (*Vr*) velocities of the plume (Fig 5) observed during the initiation stage (t<0.5 ms) indicates very different behavior between pure materials: the aluminum plume expands at both directions with the velocity ~ 3.5 - 4 m/s, whereas titanium plume has an axial expansion speed of 38 m/s and a lateral expansion speed of 9 m/s. The dissimilar joints show expansion rates close to those of titanium. In particular, the axial expansion speed increases proportionally to the beam offset from aluminum to titanium, as the higher temperatures are reached in the interaction zone due to the increase of titanium contribution.

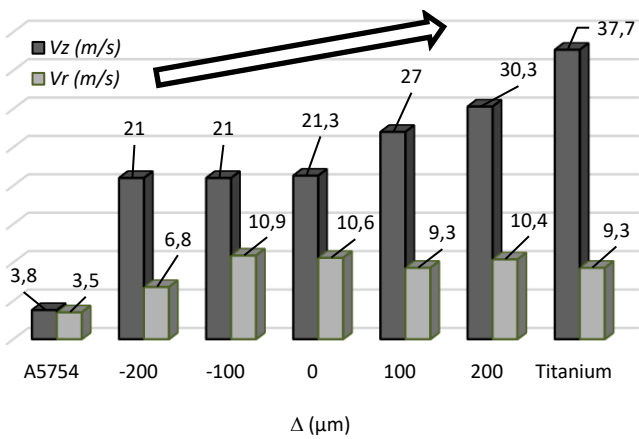

Fig. 5. Axial and radial expansion velocities during the plume initiation for standalone materials and dissimilar joints with different Δ.

3.3. Post-mortem analysis and discussion

The topography SEM images of the impact zones on the dissimilar joints (Fig 6) show in most cases the pronounced ejection of the melt and spatters toward the aluminum side, which coincides with the observed inclination of the plume. For the maximal beam offset on A5754 (-200 µm), the quasi-totality of the melted zone is situated on aluminum side. However, some melted titanium is ejected inside the melted zone in the

direction of A5754. The beam offset of -100 µm allows observing the opening of the keyhole captured by a rapid solidification of the melt. It can be seen that the keyhole opening is also inclined towards aluminum, with the right part of the melted zone rich in titanium and the left part composed by the mixture of two materials (Fig 7a). The offsets of 0 and 100 µm resulted in similar aspects of the melt, with important elongated ejections of the mixed melted zone (Fig 7b) on aluminum side. Finally, the maximal offset on titanium (200 µm) produced a particular morphology of the melted zone, where two solidification fronts can be seen (Fig 7c). In the first place, the ejection of the Ti/Al mixture on the aluminum side took place, similarly to the previous cases. But in the second place, the donut of melted titanium formed around the keyhole opening that shows no traces of inclination towards aluminum.

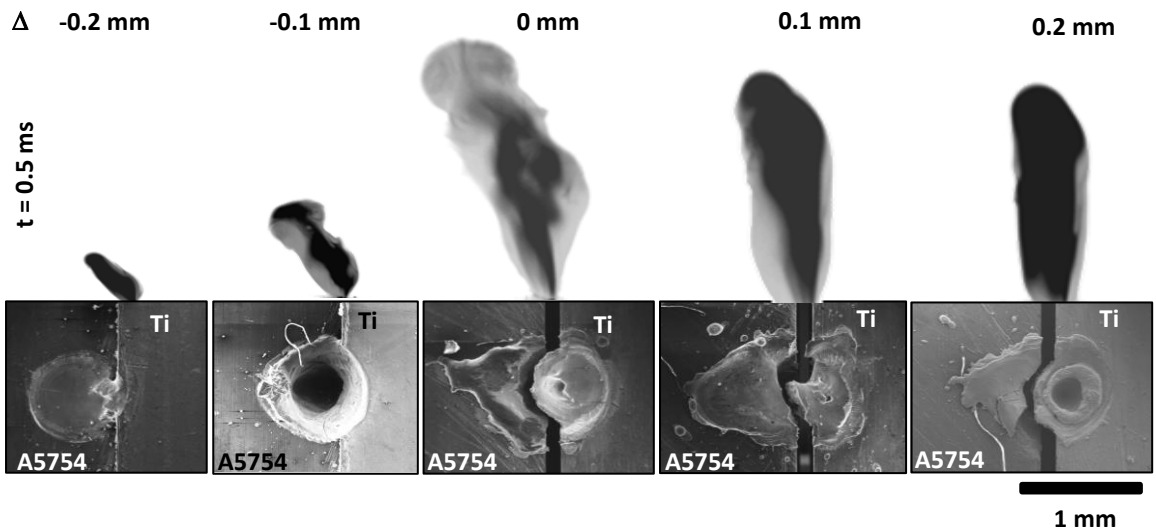

Fig. 6. The comparison of plume inclination at t=0.5 ms with the aspect of the impact zone observed by SEM.

Basing on these observations, it can be concluded that the inclination of the plume and its evolution during the pulse are closely related to the transformation of keyhole profile. The initially observed pronounced inclination of the plume on aluminum can be attributed to the preferential evaporation from titanium surface that dominates over the evaporation from the more reflective and conductive aluminum side of the joint. At the beginning of the pulse, the keyhole formation is initiated on titanium side, and the appearing curvature of the free surface makes the Ti-rich jet (perpendicular to the keyhole wall) appear inclined towards the opposite aluminum side (Fig 8a). In the same time, this powerful and hot jet contacts aluminum side of the joint, contributes to its melting and to the ejection of the mixed content of the melted zone on the surface of aluminum plate. These events correspond to the stage of plume initiation and stagnation. Then, as the joint absorbs more and more laser energy, the keyhole progresses in depth. The Ti-rich jet that could easily leave the keyhole without changing its initial direction during the previous stages, finds itself trapped inside the cylindrical keyhole (Fig 8b) and partially compensated by the vapor jet from the aluminum side. For this reason, the resulting plume visible above the keyhole opening appears more diffuse and less inclined, and the keyhole itself is not necessary inclined. Such situation takes place for the beam offsets of -100, 0 and 100 µm for the keyhole shared between titanium and aluminum (with ∅/3, ∅/2 and 2∅/3 of the beam irradiating the titanium side respectively). The case of -100 µm is particular, since the whole keyhole appears to be inclined towards aluminum side during all pulse time.

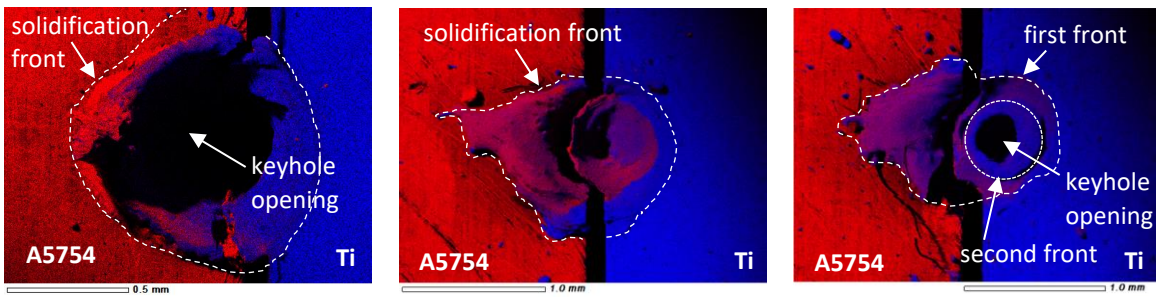

Fig. 7. X-mapping of Al (in red) and Ti (in blue) distribution in the melted zones with beam offsets of a)-100 µm, b) 0 µm and c) 200 µm.

When the beam is shifted towards titanium (200 µm offset corresponds to 5∅/6 of the beam irradiating the titanium side), the keyhole walls from all sides are mostly composed by melted titanium. And so, the opposite vaporization jets are rapidly compensated, which explains weak inclination seen only at the beginning of the pulse, which is confirmed by the presence of a second solidification front with ejected pure titanium. On the other hand, in case of beam offset on aluminum (-200 µm offset corresponds to only ∅/6 of the beam irradiating the titanium) the titanium side of the joint is situated at the periphery of the keyhole and it produces the maximal plume inclination during the evolution of the keyhole curvature in the beginning of the pulse.

In case of continuous titanium/aluminum welding, the similar dynamics of plume inclination was reported (Raja Kumar et al., 2020), however, it was repetitive due to the continuous interaction of the beam with the new portions of dissimilar joint.

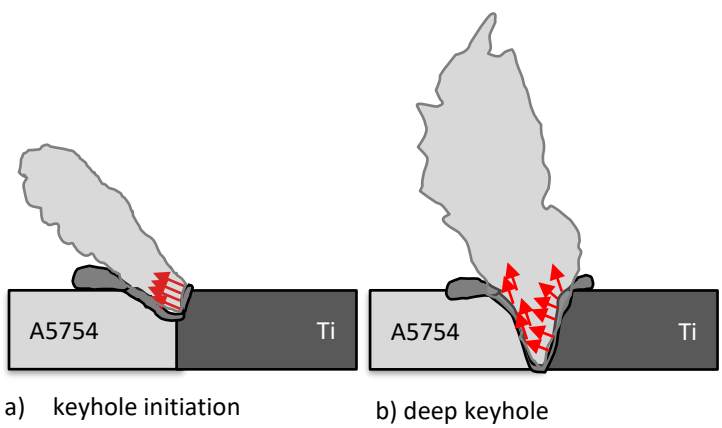

Fig. 8. The sketch of plume inclination related with the evolution of keyhole curvature (centered position of the beam, the direction of the titanium vapor jet is shown with red arrows).

4. Conclusions

The vapor plume images were treated and analyzed for the standalone materials and dissimilar A5754/titanium combinations. The spatial and temporal evolution of the vapor plumes' morphology and orientation were observed and studied. Post-mortem analysis of the melted zone was performed and correlated with results from plume image data. Some of the important conclusions drawn from this methodical approach are as follows.

- For given operational conditions, standalone aluminum produces small and dull spherical plume, since the absorbed energy is not sufficient to attain the efficient vaporization process. On the other hand, highly absorptive titanium produces bright and rapidly expanding vertical jet. Its higher luminosity can be attributed to the higher plume temperatures, as the used band-pass filter is sensitive to the thermal emission.
- The plumes formed at the dissimilar joints have brightness and dimensions close to those of titanium, since it makes the major contribution to the heat transfer in the impact zone.
- The plumes formed at the dissimilar joints are more diffuse and turbulent, because the contact with titanium induces the vaporization process on aluminum side and the resulting plume is likely to be composed by the mix of two components.
- The plumes formed at the dissimilar joints show the pronounced inclination towards aluminum side during first 1 ms of interaction, accompanied by the ejection of the melted zone and spatters on aluminum side. This inclination increases with beam offset on aluminum and rapidly decreases with beam offset on titanium.
- This initial inclination of the plume that progressively fades away with pulse duration can be attributed to the evolution of the keyhole curvature on titanium side of the dissimilar joint.

To confirm this hypothesis, further experiments need to be conducted in order to observe directly the evolution of keyhole shape, using optical coherence tomography or the observation through the transparent ceramic plate. The information on species distribution inside the plume needs to be obtained from the imaging of the plume with use of pass-band filters corresponding to the different intense lines of Ti and Al emissions. The emission spectroscopy would also provide the quantitative data about the plume temperatures that should increase with the beam offset towards titanium.

Acknowledgements

This work was supported by the region of Bourgogne Franche-Comté, by French Government and by FEDER, to which we address our sincere thanks.

References

Brock, C., Hohenstein R., Schmidt, M., 2014. Mechanisms of vapour plume formation in laser deep penetration welding, Optics and Lasers in Engineering 58, p. 93.

Huang, Y., Shen, C., Ji, X., Li, F., Zhang, Y., Hua, X., 2020. Correlation between gas-dynamic behaviour of a vapour plume and oscillation of keyhole size during laser welding of 5083 Al-alloy, Journal of Materials Processing Technology 283, 116721.

Raja Kumar, M., Jouvard, J.-M., Tomashchuk, I., Sallamand, P., 2020. Vapor plume and melted zone behavior during dissimilar laser welding of titanium to aluminum alloy, Proceedings of the Institution of Mechanical Engineers, Part L: Journal of Materials: Design and Applications 234, p. 681.

Schneider, C. A., Rasband, W. S., Eliceiri, K. W., 2012. NIH Image to ImageJ: 25 years of image analysis, Nature methods 9, p.671.

Tomashchuk, I., Mostafa, M., Caudwell, T., Sallamand, P., Duband, M., 2017. "Behavior of laser induced keyhole during dissimilar welding of metals", Lasers in Manufacturing Conference 2017, Munich, Germany.